Scripta Materialia 247 (2024) 116096

Contents lists available at ScienceDirect

Scripta Materialia

journal homepage: www.journals.elsevier.com/scripta-materialia

Stability of incommensurately modulated $Ni_{50}Mn_{27}Ga_{22}Fe_1$ 10M martensite under uniaxial tensile stress

M. Vinogradova [a,*], A. Sozinov [a], L. Straka [b], P. Veřtát [b], O. Heczko [b], M. Zelený [c], R. Chulist [d], K. Ullakko [a]

[a] Department of Physics, Materials Science Laboratory, LUT University, Lappeenranta, Finland
[b] FZU - Institute of Physics of the Czech Academy of Sciences, Prague, Czech Republic
[c] Institute of Materials Science and Engineering, Faculty of Mechanical Engineering, Brno University of Technology, Brno, Czech Republic
[d] Institute of Metallurgy and Materials Science, Polish Academy of Sciences, Krakow, Poland

ARTICLE INFO

Keywords:
Magnetic shape memory
Ni-Mn-Ga
X-ray diffraction
Incommensurately modulated crystal structure

ABSTRACT

We investigate the incommensurately modulated crystal structure in the $Ni_{50}Mn_{27}Ga_{22}Fe_1$ magnetic shape memory alloy. We focus on temperature- and stress-induced changes, particularly measuring the *a* and *b* lattice parameters and the monoclinic angle. The in-situ XRD experiment shows that the thermally-induced commensurate-incommensurate (C-IC) transition coincides with the change of the average lattice symmetry from monoclinic to orthorhombic. The thermally-induced IC structure is stable under uniaxial tensile stress along the *a*-axis for deformation $\varepsilon < 0.8$ %. A mixture of the IC and C structures appears for $\varepsilon > 0.8$ % and the changes become irreversible. The volume fraction of the C structure further increases with increasing deformation. These results provide vital initial insights into the structural evolution of Ni-Mn-Ga alloys and enable us to establish the role of C and IC structures in their extraordinarily high mobility of twin boundaries.

Ni-Mn-Ga-based alloys are prototype magnetic shape memory materials with multiple unique properties and promising applications [1–3]. Extremely low twinning stress (TS) is one of the distinctive characteristics of the Ni-Mn-Ga-based martensites [4–11]. Due to the low TS, even minor magnetic or mechanical driving forces produce giant deformation via twin boundary motion. The lattice of 10M martensite can be modulated either commensurately (C) or incommensurately (IC) [12–16]. The exact character of the modulation can be crucial given that the twin plane is the interface between two modulated twin domains. The role of C and IC modulation in extremely low twinning stress is a topic yet to be explored. Prior to such an investigation, it is essential to understand the transition between C and IC structures, especially in relation to the applied stress.

As suggested by previous investigations [17–19], the IC structure can be interpreted as composed of *a/b* nanotwins. However, the effect of stress on nanotwinned structure has not yet been addressed. To reveal this effect, we performed a tensile test of the nearly single-variant sample (with *a/b* twins) along the longest lattice direction (*a*-axis). Such loading is not expected to create and move typical twin interfaces, such as *a/c* and modulation twin boundaries [10]. The tension along the *a*-axis produces the highest shear stress in the (110) plane, which is a mirror plane for *a/b* twinning and nanotwinning. We anticipate that sufficiently high stress may induce the motion of the *a/b* nanotwin boundaries and ultimately lead to the annihilation of the IC structure.

The stress-induced effects in Ni-Mn-Ga-based alloys were studied previously for reasons such as the twin variant rearrangement [3,6,7,20–22], and martensitic and intermartensitic transformations [23,24]. Cejpek et al. [25] studied the influence of the tensile stress on the lattice parameters and modulation and pointed out the very low Young modulus of the material. In this study, our initial focus is on the previously described thermally-induced transitions. Building on these observations, we evaluate the effects of tensile deformation on IC structure, which has not been reported before.

We selected the $Ni_{50}Mn_{27}Ga_{22}Fe_1$ alloy for this study because it exhibited both 10M commensurate and 10M incommensurate martensite structures and it was possible to investigate both structures at ambient temperatures due to the thermal hysteresis [18,26]. The single crystal ingots were grown by directional solidification using [001] oriented seed crystal in AdaptaMat Ltd. Curie temperature was $T_C = 380$ K. The samples exhibited sharp martensitic transformation at $T_M = (M_s + M_f)/2 = 330$ K

* Corresponding author.
E-mail address: mariia.vinogradova@lut.fi (M. Vinogradova).

https://doi.org/10.1016/j.scriptamat.2024.116096
Received 17 January 2024; Received in revised form 5 March 2024; Accepted 22 March 2024
Available online 30 March 2024

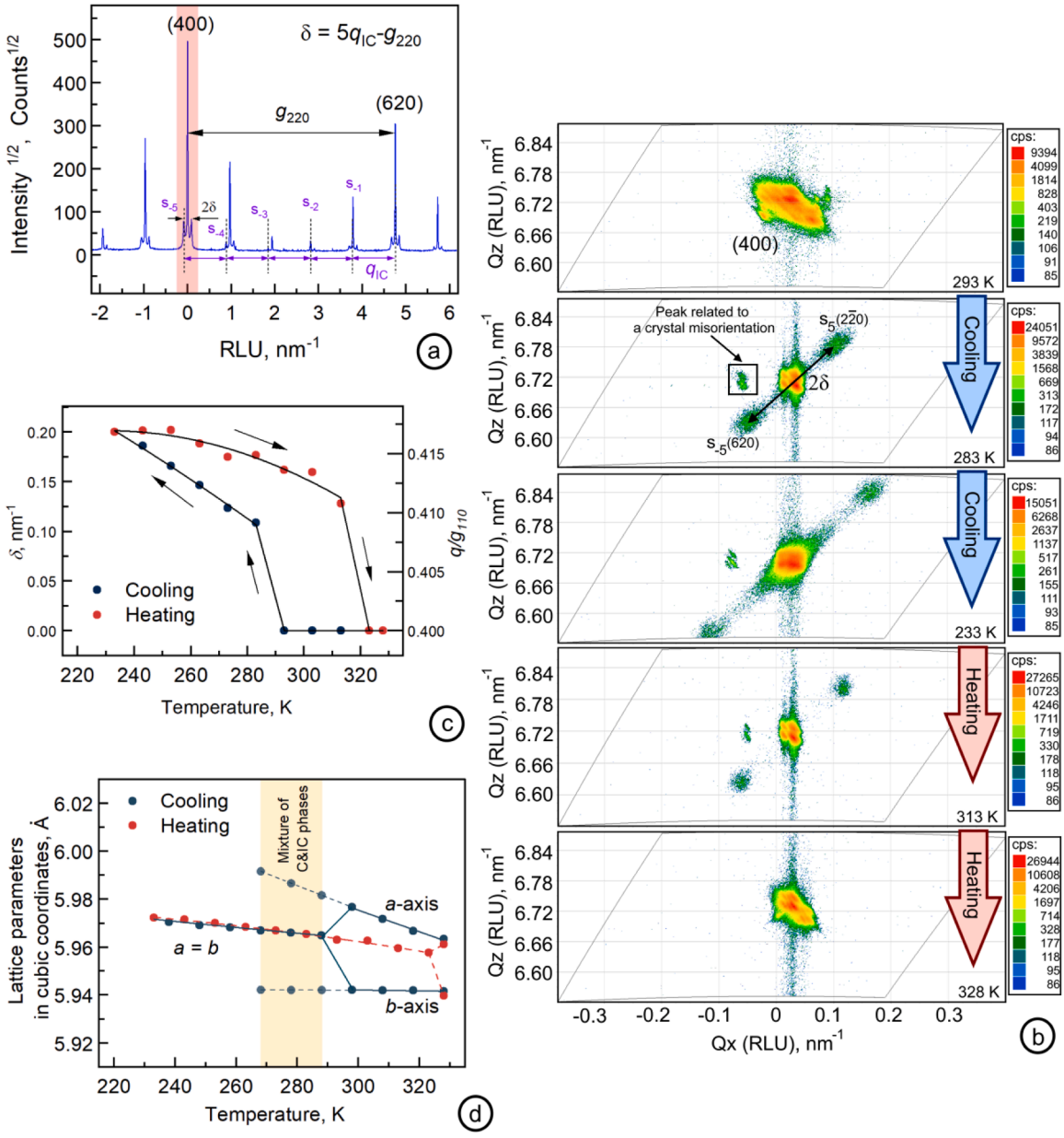

Fig. 1. Diffraction data ($Cu_{K\alpha 1}$ radiation) confirming the existence and temperature hysteresis of transition between commensurate (C) and incommensurate (IC) modulation in $Ni_{50}Mn_{27}Ga_{22}Fe_1$ alloy:
(a) Q-scan along the [110]* direction in reciprocal space. Diffraction data were recorded at $T = 293$ K after cooling to 197 K and heating back to 293 K. Satellites marked as s_{-1}, s_{-2}, s_{-3}, s_{-4}, s_{-5} are left group satellites belonging to the main peak (620). The distance between satellites $q_{IC} > 0.4$ confirms IC modulation. g_{220} is the (2, 2, 0) reciprocal lattice vector. q_{IC} is a modulation vector for incommensurate modulation. (b) Reciprocal space ultra-fast scans around the (400) reflection in the (hk0) reciprocal lattice plane showing the nearest s_5 satellites at different temperatures. $s_{-5}(620)$ and $s_5(2\bar{2}0)$ belong to the left and right satellites group correspondingly. The satellites are observed in the IC structure and disappear in the C structure. Data was obtained during cooling from 328 K to 233 K and heating back. (c) Measured temperature dependence of the half distance (δ) between the $s_{-5}(620)$ and $s_5(2\bar{2}0)$ satellites and calculated ratio of modulation vector q to reciprocal lattice vector $g_{110} = 0.5g_{220}$ using Eq. (1). (d) Temperature dependences of a- and b- lattice parameters.

and reverse transformation at $T_A = (A_s + A_f)/2 = 335$ K, where $M_s \approx M_f$, $A_s \approx A_f$ are martensite and austenite start and finish temperatures, respectively.

The nearly single-variant state of the sample with respect to the short c-axis was achieved by multiple reorientations of the c-axis in a saturated magnetic field ($\mu_0 H \sim 1$T). Finally, the short c-axis was perpendicular to the longest sample direction. X-ray diffraction proved that after such multiple reorientations, the sample had one modulation direction, i.e. there are no modulation twins. However, a/b twins still exist. The nearly single-variant state was achieved within the commensurate state. To obtain incommensurate modulation, the thermally-induced C-IC transition and its hysteresis were employed [18]. The sample was cooled down to 233 K, crossing the C-IC transition, and then heated back to room temperature. The single-variant state with respect to a/c and modulation twins remained in the resulting incommensurate state after this procedure as proven by X-ray diffraction. At the same time, X-ray diffraction demonstrates that $a = b$ making impossible macro a/b twins in the IC state (see Ref. [10] for the twinning in cubic coordinate system).

In-situ X-ray diffraction tensile experiments were performed on a bone-shape sample with a length of 10 mm and a cross-section of 0.7×2 mm^2. A custom-made deformation stage for in-situ measurements was

built from a standard linear motion stage with a micrometer. The ends of the sample were attached to the stage using strong epoxy and deformation was quantified using a micrometer. The working sample part without glue was 6.3 mm. The experiments employed two PANalytical Empyrean X-ray diffractometers, one equipped with a Cu and another with a Co tube. The Cu-based diffractometer featured a polycapillary parallel-beam lens, Anton Paar domed cooling stage DCS 500, an Eulerian cradle, and a PIXcel3D detector. Co-based diffractometer was equipped with a hybrid monochromator (parabolic mirror + double bounce Ge(220) monochromator). To mitigate the effects of crystal mosaicity or slight misorientation, ω−2θ scans were conducted in scanning line detector mode. This approach integrates contributions from slightly misoriented crystallographic domains within the detector acceptance range (3.35°). Thus the measurement is not affected by the typical 0.2–1° crystal misorientations from mosaic, which are common in Ni-Mn-Ga single crystals [7].

Fig. 1a shows a *q*-scan in the [110]* direction for the IC structure at room temperature. The scan reveals two main peaks (400) and (620) as well as modulation satellites. This observation is consistent with the data reported by Vertat et al. [18]. All satellite reflections can be indexed using a single modulation vector. Satellites of the 1st to 5th orders to the left from the (620) reflection are denoted as s_{-1} to s_{-5}. Satellites located on the right side of a main peak, in the direction of the modulation vector [110]*, are assigned positive indexes.

The distance between the satellites is equal to q_{IC} which exceeds the value of $g_{220}/5$, expected for a 10 M lattice with C modulation and $5q_{IC} = g_{220} + \delta$, where g_{220} is a reciprocal lattice vector illustrated in Fig. 1a. Given that $g_{220} = 2g_{110}$, a relationship between distances can be expressed as follows:

$$q_{IC} = g_{110}[0.4 + \delta / 5g_{110}], \quad (1)$$

which is equivalent to equations used in previous publications [12–16, 18].

Each main peak of the IC structure is between the two nearest satellites belonging to the neighboring main peaks, e.g., the (400) peak has the nearest satellites $s_{-5}(620)$ and $s_5(2\bar{2}0)$. The distance between these satellites is marked as 2δ in Fig. 1a. To verify the temperature hysteresis of the q_{IC}, as reported in [18], we measured the distance between the nearest satellites, 2δ. This was done by performing narrow reciprocal space scans of the (400) peak while cooling and heating. This method allows to observe the transitions between the structures (C or IC) faster and thus with finer temperature steps during in-situ experiments than performing full *q*-scans or larger reciprocal space mapping. The investigated range of *q*-vectors is highlighted in red in Fig. 1a. The measured maps are presented in Fig. 1b. The figures provide evidence of the temperature dependency of 2δ and, using Eq. (1), also of q_{IC}. Fig. 1c shows the hysteretic temperature dependency of the measured δ. The values q_{IC}/g_{110} were determined using Eq. (1), where g_{110} was considered constant and equal to g_{110} (293 K), since the temperature dependence of g_{110} was weak compared to the dependency of 2δ.

During cooling from 328 K to 293 K (Fig. 1b), the nearest satellites are not detected (δ = 0), and $q_{IC} = 0.4g_{110}$, indicating a commensurate modulation. Upon further cooling from 293 K to 283 K, the satellites appear and δ rises abruptly from 0 to 0.11 nm^{-1} (Fig. 1c), indicating a transition to incommensurate modulation. Further cooling leads to a smooth increase of the δ to 0.2 nm^{-1} at 233 K. Heating results in a decrease of δ to 0.128 nm^{-1} at 313 K. Rates of changing δ are different during cooling and heating. During heating from 313 K to 323 K the satellites disappear and δ changes abruptly from 0.128 to 0 nm^{-1}, manifesting that modulation became commensurate again. The observed thermal hysteresis in the δ and corresponding q_{IC}/g_{110} is in correspondence with the data presented in [18].

To sum up, our observation confirms the thermally-induced C-IC transition with decreasing temperature and its temperature hysteresis in 10 M $Ni_{50}Mn_{27}Ga_{22}Fe_1$ martensite. The magnitude of the modulation vector q_{IC} increases with decreasing temperature.

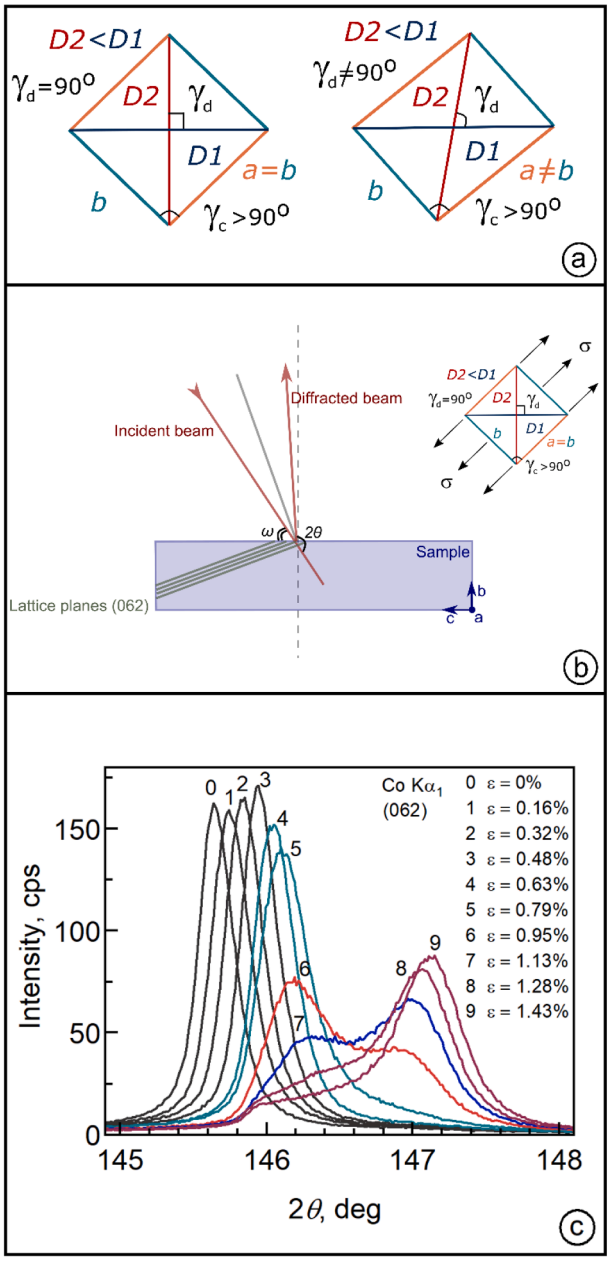

Fig. 2. Diffraction experiments on the IC sample under tensile stress. (a) Schematic representation of the sample (001) or *a*-*b* plane in two conditions. Left, is an initial orthorhombic IC crystal structure, $a = b$, $\gamma_c > 90°$, $\gamma_d = 90°$ For comparison, the right shows the C crystal structure with monoclinic symmetry. In this structure $a > b$, $\gamma_c > 90°$, $\gamma_d < 90°$ (see [19,28]). *D1* and *D2* are half of the diagonals in a parallelogram built on *a*- and *b*-axes for modulated lattices in cubic coordinates. (b) Schematic representations of the sample orientation in diffraction experiment under tensile stress *σ*. (c) Influence of applied tensile deformation on (062) peak. Splitting of the peak under tensile deformation above 0.8 % relates to the appearance and changing of volume fractions of two-state structures: the parent IC with $a = b$ and the new C with $a > b$. In the C structure, only peak (062) is observed from the two possible (602) and (062), as the long *a*-axis is preferred along the tensile stress and thus only the *b*-axis is present in the diffraction plane.

To determine the unit cell parameters of the average lattice, the diffraction pattern's modulation satellites are excluded, and only the primary reflections are considered [27], as we previously used in [28]. For conducting the measurements at different temperatures, we compressed and constrained the sample along the *c*-axis at room temperature

Table 1
Lattice parameters of C and IC crystal structures in $Ni_{50}Mn_{27}Ga_{22}Fe_1$ alloy at 293 K, given in cubic ($L2_1$-derived) and diagonal coordinates (see Ref. [28] for details).

Coordinate system	Cubic	Diagonal
Commensurate structure	$a = 5.979$ Å	$D1 = 4.229$ Å
	$b = 5.942$ Å	$D2 = 4.200$ Å
	$c = 5.572$ Å	$c = 5.572$ Å
	$\gamma_c = 90.39°$	$\gamma_d = 89.64°$
Incommensurate structure	$a = b = 5.963$ Å	$D1 = 4.231$ Å
	$c = 5.572$ Å	$D2 = 4.202$ Å
	$\gamma_c = 90.39°$	$c = 5.572$ Å
		$\gamma_d = 90°$

to simplify variant microstructure (see detail in [28]). Nevertheless, the sample still contained *a/b* twins in the C state. Thus, the direct determination of the *a*- and *b*-lattice parameters using 2θ angles of (400) and (040) in 10 M martensite could be problematic due to the peak overlap originating from this *a/b*-twinning [17]. To improve the accuracy, we derived the lattice parameters from 2θ for (602), (062) and (004) peaks, where the 2θ angle for the former two is significantly higher and there are no overlaps. The used peaks, similarly to (400) and (040), do not depend on lattice monoclinic distortion, thus the lattice parameter calculation is straightforward.

Temperature dependences of lattice parameters *a* and *b* are shown in Fig. 1d. At 328 K, the lengths of lattice parameters *a* and *b* differ, $a > b$. During cooling the difference between *a*- and *b*- parameters further increases. A third peak, emerging between the original (602) and (062) at 288 K, grows in intensity within the range 288–268 K. Simultaneously, intensities of the original peaks decrease, and they vanish at 258 K.

In the nanotwinning model, the concurrent presence of these three diffraction peaks was attributed to an intermediate state, characterized by a mixture of coarse microtwins and nanotwins [17,19]. Using a more conventional approach, the behavior of the intensities of the peaks can be interpreted as the transition between two states C ($a > b$) and IC ($a = b$) with a region of coexistence (C + IC) [29,30]. Upon heating from 218 K, a single peak persists up to 323 K, implying that the alloy has equal lattice parameters *a* and *b* after cooling over a wide temperature range.

Additionally, we measured the temperature dependencies of the short *c*-axis and 2θ angles for (444) and ($\bar{4}44$) peaks, whose difference directly relates to the lattice monoclinic angle γ_c as presented in Ref. [28]. The *c*-axis length increases with increasing temperature. The cooling and heating curves match in all temperature range, with no hysteresis. The 2θ difference of the (444) and ($\bar{4}44$) peaks positions and corresponding monoclinic distortion decreases with increasing temperature. Temperature dependences are again smooth and show no hysteresis.

Thus, there is no hysteresis in the thermal evolution of the *c*-axis and the lattice monoclinicity γ_c. In contrast, the lengths of the *a*- and *b*-axis exhibit thermal hysteresis, which correlates with the thermal hysteresis observed in modulation vector magnitude q_{IC}, Fig. 1c. This difference can be explained by the different symmetries of the average lattices of the C and IC structures [12], see Fig. 2a. Symmetry of C structure is monoclinic with $a > b$, $\gamma_c > 90°$, and $\gamma_d \neq 90°$, where γ_d is an angle between diagonals in the parallelogram build using the lattice parameters *a* and *b*, Fig. 2a, also see Ref. [28]. The IC structure is orthorhombic and – despite that angle $\gamma_c \neq 90°$ is the same as in the C structure – the $a = b$ (Fig. 1d) implies $\gamma_d = 90°$ [17,19,28]. The different lattice symmetries enable the simultaneous existence of thermal hysteresis in the *a*- and *b*- axes together with no thermal hysteresis for the *c*-axis and monoclinicity γ_c upon C-IC-C transition.

Summarizing the thermally induced effects, we observe a C-IC-C transition with a large thermal hysteresis. The lattice parameters for both structures are presented in Table 1. While the C structure exhibits a monoclinic symmetry, the IC structure is orthorhombic. Consequently, the C-IC transition results not only in the change of modulation vector but simultaneously also in the apparent merging of different *a* and *b* axes

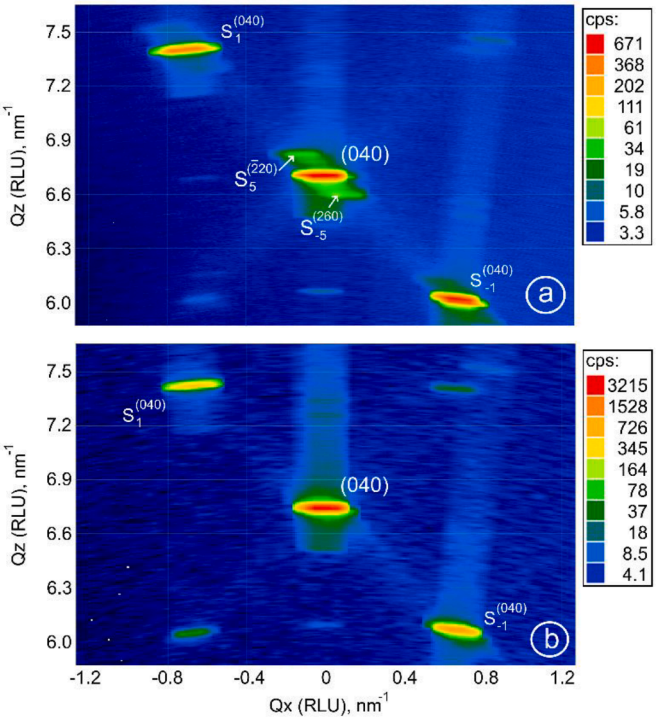

Fig. 3. Reciprocal space map around the (040) reflection in the (hk0) reciprocal lattice plane. Data are obtained with Cu radiation and a polycapillary X-ray lens in the incident beam optics (without a monochromator).
(a) Sample in initial state without deformation, $\varepsilon = 0$ %. The $s_1(040)$, $s_{-1}(040)$, $s_{-5}(260)$, and $s_5(2\bar{2}0)$ satellites are visible, indicating the IC modulation state. Other less intensive peaks (not marked) are related to the absence of a monochromator and a small volume fraction of the second modulation domain in the sample. (b) Sample under tensile $\varepsilon = 1.43$ %. The $s_{-5}(260)$ and $s_5(2\bar{2}0)$ satellites vanish, providing evidence of the transition from the IC to the C modulation state during the tensile deformation.

((602) and (062) peaks) into a single unified length $a = b$, evidenced by the single central peak. Previously, the evolution of the peaks was explained by the nanotwinning of the lattice but it can also be interpreted as a transition between C and IC structures, with a region of coexistence C + IC. Further tensile experiments exploit the fact that the structure can be either commensurate or incommensurate at the ambient temperature.

To assess the stability of the IC structure, we conducted a tensile test involving load-unload cycles on a single-variant IC sample, applying stress along the longest lattice direction, the *a*-axis. Such loading is not expected to result in the *a/c* or modulation twin boundary motion [10] but can stimulate the motion of the *a/b* nanotwin boundaries with the twinning plane (110) and ultimately lead to the disappearance of the IC structure. As the applied stress was not measured in our experiment no stress-strain curve is available. However, the stress-strain curve of similar material with commensurate modulation was published by Cejpek et al. [25], which indicates the exceptionally small Young's modulus of 10M martensite along the *a*-axis.

We utilized changes in the diffraction line position, specifically the 2θ angle, under tension, to probe deformation in several directions approximately perpendicular to the *a*-axis. We found that the direction of normal to the plane (062) was suitable for such investigation of bulk single crystal. It was less than 20° away from the direction of the "*b*"-axis but had a higher 2θ angle than the other planes used for the measurements (044) and (060). Plane (060) also had a high 2θ angle, but its intensity was much smaller compared to the (062) line. Fig. 2b shows schematically the sample orientation in our diffraction experiment under tensile stress. Parallel beam X-ray optics with a monochromatic $Co_{K\alpha 1}$ radiation were

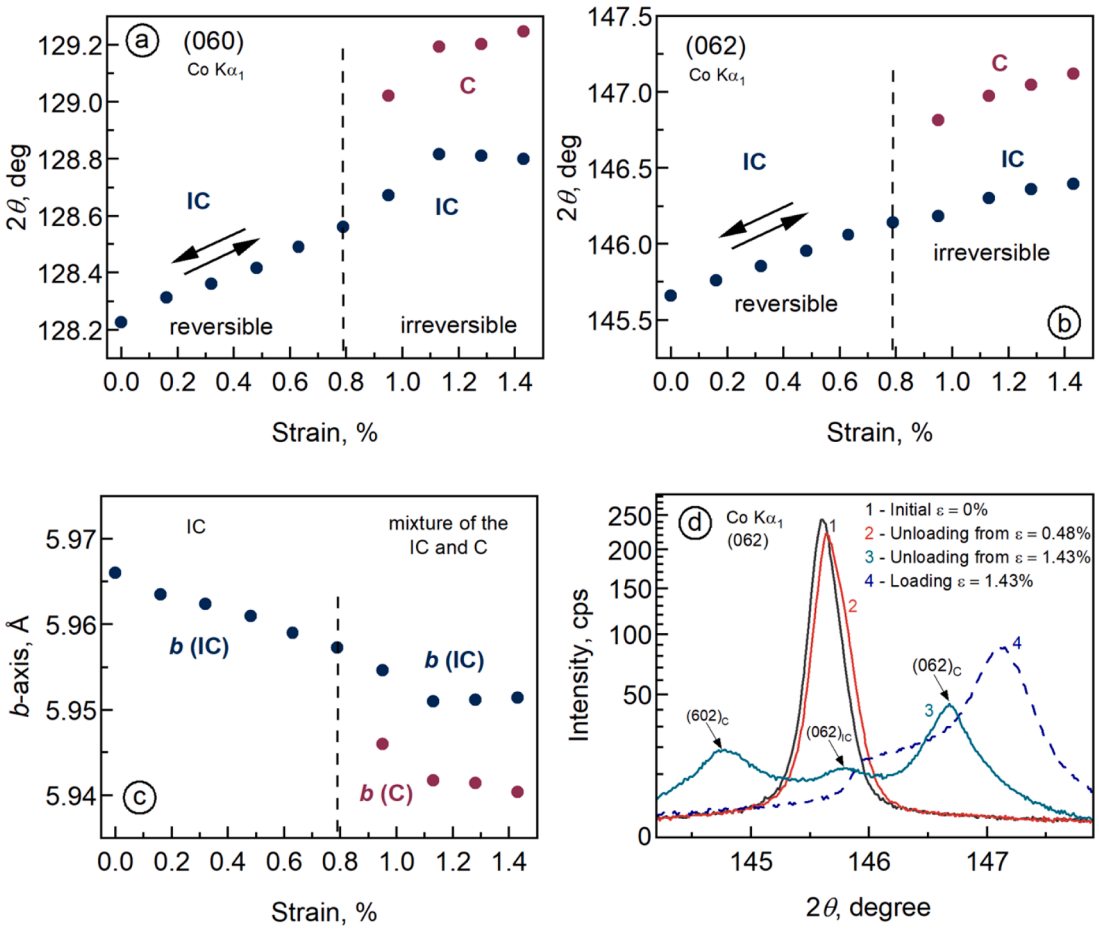

Fig. 4. (a)-(b) 2θ-angle vs. strain for (060) and (062) peaks. (c) Length of *b*-axis vs. strain. (d) Diffraction patterns near the (062) peak at different sample conditions (1) 0 % of deformation; (2) after loading to 0.48 % deformation and unloading to almost 0 %; (3) after loading up to 1.43 % deformation and unloading to almost 0 %. The peak positions for C and IC structures correspond to the following lattice parameters: $a_C = 5.981$ Å, $b_C = 5.946$ Å, $a_{IC} = b_{IC} = 5.962$ Å. These parameters are close to the data presented in Table 1. (4) upon loading to 1.43 % deformation.

utilized to decrease the sensitivity of 2θ angle on the sample displacement and to increase the 2θ angle in comparison to Cu radiation. As shown in Fig. 2c, the (062) 2θ angle is greater than 145°, allowing us to detect very small changes in lattice spacing and the peak splitting is correspondingly better resolved.

Reciprocal space mapping was performed to probe directly which structure (C or IC) is in the sample under tensile stress. Fig. 3 shows the (040) peak with the nearest satellites at different deformations. At the initial state ($\varepsilon = 0$ %), there are two $s_{-5}(620)$ and $s_5(2\bar{2}0)$ satellites near the (040) peak, confirming the presence of the IC structure. When the sample is deformed to $\varepsilon = 1.43$ %, these satellites disappear (Fig. 3b). Only the $s_{-1}(040)$ and $s_1(2\bar{2}0)$ satellites remain, marking the progressing transition to the C structure.

Fig. 4 displays how the 2θ position of (060) and (062) peaks vary as a function of deformation along the *a*-axis, and alongside the calculated *b*-axis length is shown. Deformation ε along *a*-axis was determined from micrometer reading and sample length. Loading above $\varepsilon > 0.8$ % leads to the emergence of a new peak located at a higher 2θ-angle (for both (060) and (062) peaks). We conclude that this peak is related to the *b*-axis of the emerging C monoclinic state (Fig. 1d). Length of the *b*-axis in the C monoclinic state is shorter than the $b = a$ axis in the IC orthorhombic structure. The new peak, together with the initial peak, continues to shift to a higher 2θ-angle with increasing deformation. Figs. 2c, 4a, b, c illustrate that the two-state structure (C + IC) exists in the broad range of deformation above $\varepsilon > 0.8$ %. The volume fraction of the monoclinic C state increases with deformation on account of the IC orthorhombic state, as demonstrated by the peak intensity redistribution in Fig. 2c.

The loading-unloading cycles up to deformation $\varepsilon = 0.8$ % are reversible and result in the same 2θ peak positions at $\varepsilon = 0$ prior to and after loading (Fig. 4d). The orthorhombic symmetry remains, thus the strain level to modify the IC structure is above 0.8 % deformation. Unloading from the deformation exceeding $\varepsilon = 0.8$ % is not reversible (Fig. 4d). The unloaded state consists of a mixture of both C and IC domains. During the unloading from the deformation above $\varepsilon = 0.8$ % the split peaks found at high levels of deformation (Fig. 2c) shift to smaller 2θ angles. At an almost unloaded state, the third peak emerges from the left side of the initial peaks (Fig. 4d). These three peaks correspond to different *a*- and *b*-axes in the C state and one (central) peak in the IC state due to $a = b$. The indexation and positions of the peaks are shown in Fig. 4d. The calculated *a*- and *b*-axis lengths correspond to the lattice parameters of the C and IC structures given in Table 1, with small deviations caused by the incomplete unloading. Two peaks in the C structure indicate the appearance of usual *a*/*b* twin domains in the unloaded state.

In summary, we explored the stability of the incommensurately modulated crystal structure in the $Ni_{50}Mn_{27}Ga_{22}Fe_1$ magnetic shape memory alloy under uniaxial tensile stress. Emphasizing the temperature- and stress-induced changes, the investigation focused on measuring the *a* and *b* lattice parameters and the monoclinic angle. Key findings are:

I. The thermally-induced commensurate-incommensurate (C-IC) transition coincides with a transformation from monoclinic to orthorhombic lattice symmetry.

II. The IC structure maintains stability under uniaxial tensile stress along the *a*-axis until deformation of $\varepsilon = 0.8$ %. Beyond this threshold, a mixture of IC and C structures emerges, with the C structure becoming more predominant as deformation increases.

This study provides significant insights into the structural evolution of Ni-Mn-Ga alloys, particularly in relation to tensile deformation. It establishes the role of C and IC structures in the material's response to mechanical forces. Based on our results and phase diagram presented in Ref. [17] we suggest that material with extremely low twinning stress such as reported in [9] should have IC modulation. This points out that the investigation of the physical properties of the IC structure is principal for the MSM field.

Declaration of competing interest

The authors declare that they have no known competing financial interests or personal relationships that could have appeared to influence the work reported in this paper.

Acknowledgments

This work was financially supported by the Academy of Finland (grant number 325910). The authors from the Czech Republic acknowledge the funding from the Czech Science Foundation grant no. 21-06613S and the assistance provided by the Ferroic Multifunctionalities project, supported by theYouth, and Sports of the Czech Republic, Project No. CZ.02.01.01/00/22_008/0004591, co-funded by the European Union. The international mobility of Alexei Sozinov was supported by ESIF and MEYS project MOBILITY FZU 2 – CZ.02.2.69/0.0/0.0/18_053/0016627. Robert Chulist acknowledges the projects 2021/42/E/ST5/00367 of the National Science Centre of Poland.

References

[1] J.P. Liu, E. Fullerton, O. Gutfleisch, D.J. Sellmyer, Nanoscale Magnetic Materials and Applications, Springer US, Boston, MA, 2009, https://doi.org/10.1007/978-0-387-85600-1.
[2] M. Acet, Ll. Mañosa, A. Planes, Magnetic-field-induced effects in martensitic Heusler-based magnetic shape memory alloys, Handb. Magn. Mater. (2011) 231–289, https://doi.org/10.1016/B978-0-444-53780-5.00004-1.
[3] I. Aaltio, A. Sozinov, Y. Ge, K. Ullakko, V.K. Lindroos, S.P. Hannula, Giant magnetostrictive materials, in: S. Hashmi (Ed.), Ref. Module Mater. Sci. Mater. Eng., Elsevier, 2016, https://doi.org/10.1016/B978-0-12-803581-8.01830-0. B9780128035818019000.
[4] L. Straka, H. Hänninen, A. Soroka, A. Sozinov, Ni-Mn-Ga single crystals with very low twinning stress, J. Phys. Conf. Ser. 303 (2011) 012079, https://doi.org/10.1088/1742-6596/303/1/012079.
[5] O. Heczko, A. Sozinov, K. Ullakko, Giant field-induced reversible strain in magnetic shape memory NiMnGa alloy, IEEE Trans. Magn. 36 (2000) 3266–3268, https://doi.org/10.1109/20.908764.
[6] M. Chmielus, K. Rolfs, R. Wimpory, W. Reimers, P. Müllner, R. Schneider, Effects of surface roughness and training on the twinning stress of Ni–Mn–Ga single crystals, Acta Mater. 58 (2010) 3952–3962, https://doi.org/10.1016/j.actamat.2010.03.031.
[7] D. Musiienko, F. Nilsén, A. Armstrong, M. Rameš, P. Veřtát, R.H. Colman, J. Čapek, P. Müllner, O. Heczko, L. Straka, Effect of crystal quality on twinning stress in Ni–Mn–Ga magnetic shape memory alloys, J. Mater. Res. Technol. 14 (2021) 1934–1944, https://doi.org/10.1016/j.jmrt.2021.07.081.
[8] J. Wang, H. Sehitoglu, Twinning stress in shape memory alloys: theory and experiments, Acta Mater. 61 (2013) 6790–6801, https://doi.org/10.1016/j.actamat.2013.07.053.
[9] O. Heczko, V. Kopecký, A. Sozinov, L. Straka, Magnetic shape memory effect at 1.7 K, Appl. Phys. Lett. 103 (2013) 072405, https://doi.org/10.1063/1.4817941.
[10] L. Straka, O. Heczko, H. Seiner, N. Lanska, J. Drahokoupil, A. Soroka, S. Fähler, H. Hänninen, A. Sozinov, Highly mobile twinned interface in 10 M modulated Ni–Mn–Ga martensite: analysis beyond the tetragonal approximation of lattice, Acta Mater. 59 (2011) 7450–7463, https://doi.org/10.1016/j.actamat.2011.09.020.
[11] A. Saren, A. Sozinov, S. Kustov, K. Ullakko, Stress-induced a/b compound twins redistribution in 10 M Ni-Mn-Ga martensite, Scr. Mater. 175 (2020) 11–15, https://doi.org/10.1016/j.scriptamat.2019.09.001.
[12] L. Righi, F. Albertini, L. Pareti, A. Paoluzi, G. Calestani, Commensurate and incommensurate "5M" modulated crystal structures in Ni–Mn–Ga martensitic phases, Acta Mater. 55 (2007) 5237–5245, https://doi.org/10.1016/j.actamat.2007.05.040.
[13] L. Righi, F. Albertini, A. Paoluzi, S. Fabbrici, E. Villa, G. Calestani, S. Besseghini, Incommensurate and commensurate structural modulation in martensitic phases of FSMA, Mater. Sci. Forum 635 (2009) 33–41, https://doi.org/10.4028/www.scientific.net/MSF.635.33.
[14] A. Çakır, M. Acet, L. Righi, F. Albertini, M. Farle, Characteristics of 5 M modulated martensite in Ni-Mn-Ga magnetic shape memory alloys, AIP Adv. 5 (2015) 097222, https://doi.org/10.1063/1.4932233.
[15] S.O. Mariager, T. Huber, G. Ingold, The incommensurate modulations of stoichiometric Ni2MnGa, Acta Mater. 66 (2014) 192–198, https://doi.org/10.1016/j.actamat.2013.11.077.
[16] T. Fukuda, H. Kushida, M. Todai, T. Kakeshita, H. Mori, Crystal structure of the martensite phase in the ferromagnetic shape memory compound Ni2MnGa studied by electron diffraction, Scr. Mater. 61 (2009) 473–476, https://doi.org/10.1016/j.scriptamat.2009.04.046.
[17] L. Straka, J. Drahokoupil, P. Veřtát, M. Zelený, J. Kopeček, A. Sozinov, O. Heczko, Low temperature a/b nanotwins in Ni50Mn25+xGa25−x Heusler alloys, Sci. Rep. 8 (2018) 11943, https://doi.org/10.1038/s41598-018-30388-8.
[18] P. Veřtát, H. Seiner, L. Straka, M. Klicpera, A. Sozinov, O. Fabelo, O. Heczko, Hysteretic structural changes within five-layered modulated 10 M martensite of Ni–Mn–Ga(–Fe), J. Phys. Condens. Matter 33 (2021) 265404, https://doi.org/10.1088/1361-648X/abfb8f.
[19] L. Straka, J. Drahokoupil, P. Veřtát, J. Kopeček, M. Zelený, H. Seiner, O. Heczko, Orthorhombic intermediate phase originating from {110} nanotwinning in Ni50.0Mn28.7Ga21.3 modulated martensite, Acta Mater. 132 (2017) 335–344, https://doi.org/10.1016/j.actamat.2017.04.048.
[20] J.M. Ball, C. Chu, R.D. James, Hysteresis during stress-induced variant rearrangement, J. Phys. IV 05 (1995), https://doi.org/10.1051/jp4:1995834. C8-245-C8-251.
[21] P. Müllner, Stress-induced twin rearrangement resulting in change of magnetization in a Ni–Mn–Ga ferromagnetic martensite, Scr. Mater. 49 (2003) 129–133, https://doi.org/10.1016/S1359-6462(03)00219-7.
[22] P. Molnar, P. Sittner, P. Lukas, S.-P. Hannula, O. Heczko, Stress-induced martensite variant reorientation in magnetic shape memory Ni–Mn–Ga single crystal studied by neutron diffraction, Smart Mater. Struct. 17 (2008) 035014, https://doi.org/10.1088/0964-1726/17/3/035014.
[23] V.V. Martynov, X-ray diffraction study of thermally and stress-induced phase transformations in single crystalline Ni-Mn-Ga alloys, J. Phys. IV 05 (1995), https://doi.org/10.1051/jp4:1995810. C8-91-C8-99.
[24] V.A. Chernenko, E. Villa, D. Salazar, J.M. Barandiaran, Large tensile superelasticity from intermartensitic transformations in Ni49Mn28Ga23 single crystal, Appl. Phys. Lett. 108 (2016) 071903, https://doi.org/10.1063/1.4942195.
[25] P. Cejpek, D. Drozdenko, K. Mathis, R.H. Colman, M. Dopita, L. Straka, O. Heczko, Exceptionally small Young modulus in 10 M martensite of Ni-Mn-Ga exhibiting magnetic shape memory effect, Acta Mater. 257 (2023) 119133, https://doi.org/10.1016/j.actamat.2023.119133.
[26] M. Klicpera, N. Biniskos, L. Cañadillas-Delgado, P. Cejpek, R. Chulist, O.R. Fabelo Rosa, P. Veřtát, Solving structure of five-layered modulated martensite of Ni-Mn-Ga(-Fe) using single-crystal neutron diffraction. (2023). https://doi.org/10.5291/ILL-DATA.DIR-299.
[27] P.M. de Wolff, The pseudo-symmetry of modulated crystal structures, Acta Crystallogr. Sect. A 30 (1974) 777–785, https://doi.org/10.1107/S0567739474010710.
[28] M. Vinogradova, A. Sozinov, L. Straka, P. Veřtát, O. Heczko, M. Zelený, R. Chulist, E. Lähderanta, K. Ullakko, Constant plane shift model: structure analysis of martensitic phases in Ni50Mn27Ga22Fe1 beyond non-modulated building blocks, Acta Mater. 255 (2023) 119042, https://doi.org/10.1016/j.actamat.2023.119042.
[29] L. Straka, J. Drahokoupil, O. Pacherová, K. Richterová, V. Kopecký, H. Hänninen, O. Heczko, Thermally induced changes of structure in Ni50Mn25+xGa25−x magnetic shape memory single crystals with very low twinning stress, (2014). https://doi.org/10.48550/arXiv.1411.1550.
[30] P. Veřtát, L. Straka, J. Drahokoupil, O. Heczko, Study of 10M' nanotwinned phase in the vicinity of martensitic transformation in Ni-Mn-Ga Magnetic shape memory alloy, Acta Phys. Pol. A 134 (2018) 859–862, https://doi.org/10.12693/APhysPolA.134.859.